Journal of Molecular Structure 1346 (2025) 143220

Contents lists available at ScienceDirect

Journal of Molecular Structure

journal homepage: www.elsevier.com/locate/molstr

Synthesis, comprehensive characterization, crystallographic and density functional theory (DFT) studies of tridentate amic acid compounds

Nonkosi Matinise [a], Claire Ineza [a], Segun D. Oladipo [a], Nusrat M. Begum [a], Abosede A. Badeji [b], Anton S. Lopis [c], Robert C. Luckay [a,*]

[a] Department of Chemistry and Polymer Science, Stellenbosch University, Private Bag X1, Matieland, Stellenbosch, 7602, South Africa
[b] Department of Chemical Sciences, Tai Solarin University of Education, Ijagun, Ogun State, Nigeria
[c] Centre for High Performance Computing, CSIR, 15 Lower Hope Street, Rosebank, Cape Town 7700, South Africa

ARTICLE INFO

Keywords:
Amic acid ligands
Tridentate coordination compounds
Density functional theory (DFT) calculations
Cu(II) complexes
Crystal structures
Spectroscopic characterization (FTIR, NMR, MS)
Structure–property relationships

ABSTRACT

Amic acids constitute a class of organic acids which have both carboxylic as well as amide functional groups within their structure and their synthesis has gained significant interest due to their applications in medicine and hydrometallurgical industries. In this study, a series of novel tridentate amic acid-based ligands were synthesized via a bimolecular nucleophilic substitution (SN_2) reaction between 2-chloro-N,N-dioctylacetamide and glycine derivatives to afford (2-(dioctylamino)-2-oxoethyl)glycine (**L1**), N-(2-(dioctylamino)-2-oxoethyl)-N-methyl-glycine **(L2),** N-(2-(dioctylamino)-2-oxoethyl)-N-ethylglycine **(L3)**, N-(2-(dioctylamino)-2-oxoethyl)-N-iso-butylglycine (**L4**) and (2-(dihexylamino)-2-oxoethyl) methylglycine **(L5)**. Structural modifications were introduced by varying the alkyl substituents on the central amine nitrogen to investigate their influence on coordination behaviour. Ligands **L1** – **L5** were characterized using various spectroscopic techniques such as FT-IR ATR, NMR (^{1}H and ^{13}C), together with mass spectrometry to confirm their successful synthesis. The diagnostic peak for the methylene protons in the region of (3.8–4.0) ppm in the ^{1}H NMR spectra corroborates the formation of a new bond between the amino acid moiety and the amide carbonyl carbon across all compounds. To further validate the coordination properties of these ligands, copper(II) complexes of two representative ligands (**L2** and **L5**) were obtained and structurally characterized using single-crystal X-ray diffraction. The crystal structures of copper(II) complexes of **L2** and **L5** which adopt the general molecular formula of **Cu(L2)$_2$** and **Cu(L5)$_2$** also affirm the successful synthesis of the tridentate amic acids. These are the first reported crystal structures of copper complexes involving tridentate amic acid extractants. The complexes adopt a distorted octahedral geometry with the Cu^{2+} ion coordinated by two ligands in a tridentate fashion—through carboxylic, amide, and amine donor atoms—resulting in four five-membered chelate rings per complex Notably, the observed bite angles were smaller than 90°, indicating a constrained coordination environment and supporting a distorted geometry. To complement the experimental findings, Density Functional Theory (DFT) calculations at B3LYP (Becke-Lee-Yang-Parr) method with the LANL2DZ and 6–31 G (d, p) basis set were performed to model the electronic and structural properties of the ligands and their Cu(II) complexes. The calculations not only corroborated the crystallographic bond lengths and angles but also highlighted the role of alkyl substituent sterics and electronics in modulating complex stability. The results showed that electron-donating alkyl chains affect the bond metrics at the amine nitrogen, which in turn influences the metal-binding cavity and stability of the resulting complex. Overall, this work provides the first comprehensive correlation between synthetic, spectroscopic, crystallographic, and theoretical data for this class of ligands. It establishes a foundation for tailoring amic acid ligands with improved selectivity and efficiency for base metal ion separation.

1. Introduction

Tridentate amic acid ligands have gained popularity in recent years due to their affordability and environmental sustainability, with the aim of setting up a new waste-free oxidation method at the industry level [1]. These “green ligands” are made of amino acids, which only contain four

* Corresponding author.
E-mail address: rcluckay@sun.ac.za (R.C. Luckay).

https://doi.org/10.1016/j.molstruc.2025.143220
Received 26 May 2025; Received in revised form 24 June 2025; Accepted 3 July 2025
Available online 5 July 2025

elements: carbon(C), hydrogen(H), oxygen(O), and nitrogen(N). Therefore, they offer significant properties when compared to commercially used organophosphorus extractants [2,3], refer to the list below:

(1) because there are no Phosphorus (P) or Sulphur (S) elements in their structure, they are biodegradable and help to reduce the product's pollutants.; (2) they expand solvent options for solvent extraction with their excellent solubility in a wide range of organic solvents such as kerosene, dodecane, and ionic liquids; and (3) due to the broad spectrum of amino acids, the extraction performance by amic acid extractants is presumed to be flexible [4,5], allowing accurate control over the physical and chemical properties of specific targets(metal ions). (4) their straightforward synthesis allows for a simple bimolecular nucleophilic substitution reaction to produce the extractant in moderate yields under mild conditions.

Tridentate amic acid ligands are extensively used for the separation and recycling of numerous strategic metal ions, owing to their advantageous properties. Several studies, including Baba et al. [6,7], have revealed excellent extraction performance using these amic acid-type ligands. They successfully developed D2EHAG, a new ligand with metal selectivity in the following order: Ni^{2+} follows Co^{2+} and then Mn^{2+}. D2EHAS demonstrated a similar extraction behaviour to D2EHAG, achieving the separation of Ni^{2+} and Co^{2+} from Mn^{2+} at lower pH values compared to D2EHAG under similar experimental conditions. However, the selectivity for Ni^{2+} over Co^{2+} was less noticeable with D2EHAS.

Ni(II) and Co(II) can be separated from Mn(II) with high efficiency and selectivity using amic-acid ligands, which eliminate the need for extra salts or the use of more ligands. The separation of Ni(II) and Co(II) using amic-acid ligands can be easily accomplished with dilute sulfuric acid, eliminating the need for high-temperature, concentrated hydrochloric acid stripping, in contrast to commercial thiophosphinic acid ligands or synergistic extraction systems involving oximes and carboxylates, which preferentially extract Ni(II) and Co(II) over Mn(II) [8].

While previous studies have demonstrated the effective use of amic acid-type ligands in separating base metals, little attention has been paid to the influence of alkyl substituent variation on the central nitrogen atom, a feature that can significantly impact steric hindrance, electron density, and overall metal-binding behaviour. Moreover, to date, no crystal structures of metal complexes involving tridentate amic acid extractants have been reported in the Cambridge Structural Database, representing a substantial gap in the understanding of their solid-state coordination chemistry.

Three coordination sites are present in these ligands: carboxylic, amide, and amine groups. As shown in *Fig. 1*, the strength of the bond between the metal ion and the central amine group largely determines how well these extractants separate metal ions.

Therefore, considering all the above-mentioned properties of amic acid extractants for selective separation in solvent extraction. We opt to develop new ligands by varying the length or bulkiness of an alkyl chain attached to the central nitrogen (N) atom as this N atom is believed to contribute to the extraction efficiency of metal ions and coordination to the metal centre.

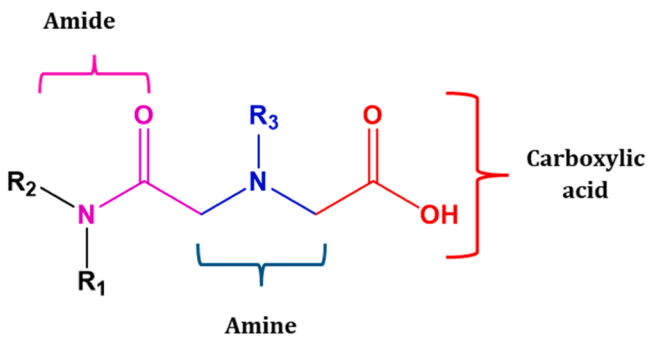

Fig. 1. General structure of tridentate amic acid type extractants.

In this context, the present study aims to discuss in detail the design and synthesis of a series of novel tridentate amic acid-based ligands by systematically varying the *n*-alkyl substituents to modulate their steric and electronic properties. These ligands were characterized through a combination of spectroscopic techniques and mass spectrometry. Furthermore, to gain deeper insights into their coordination modes and structure–property relationships, single-crystal X-ray diffraction studies were conducted on their Cu(II) complexes, marking the first crystallographic evidence of amic acid extractants in metal coordination.

Designing new materials with specific properties to tailor their structure for a particular application requires in-depth consideration of the properties of the discrete components, their response to chemical modification, in addition to their chemical and physical interactions of the crystalline solid at the molecular level. Laboratory experiments can be limited by various interferences, hindering the understanding of atomic systems at the molecular level. DFT calculations offer valuable modelling tools to investigate material properties under extreme conditions, overcoming these experimental limitations.

DFT is a computational quantum mechanical modelling method used in physics, material science and chemistry to investigate the electronic structures of almost any kind of atomic system; atoms, molecules, and crystals just to name a few [9,10]. These calculations are specifically based on the electron probability density function designated by $\rho(x, y, z)$, not a wave function. Even though the approach of wave function extends a greater accuracy, it is somewhat computationally expensive due to the inclusion of correlation effects. This integrated experimental–computational approach allows for the rationalization of ligand design strategies for improved metal selectivity and extraction efficiency.

While some may argue that comparing solid-state and solution-based studies is challenging, it provides valuable fundamental information. Technically speaking from a synthetic chemist's perspective, crystallization from solutions entails isolating the solid that was synthesized in solution. Therefore, it only makes sense to combine solid-state, computational, and solution-based studies for comprehensive understanding. The computational chemistry studies were used to rationalize the relationship of the bond lengths for each ligand structure and compare how these bond lengths are similar to literature.

This work presents a novel class of eco-friendly ligands with well-defined coordination geometries and provides a comprehensive understanding of how ligand structure influences metal complexation. These findings pave the way for future applications in sustainable metal recovery and green separation technologies.

2. Experimental section

2.1. Reagents and chemicals

2-Chloroacetyl chloride, dihexylamine, dioctylamine, ethylamine, glyoxylic acid monohydrate, isobutylamine, and sodium hydroxide were bought from Sigma-Aldrich (Pty) Ltd. Glycine, methylglycine and sodium sulphate (anhydrous)were purchased from Merck (Pty) Ltd. Dichloromethane, diethyl ether, hydrochloric acid solution, and methanol were supplied by KIMIX Chemical and lab Supplies (CC). All chemicals were used without any further purification.

2.2. Instrumentation

A Nicolet Avatar 330 FT-IR spectrometer was used to acquire Fourier Transform Infrared (FTIR) spectra of both solid and oil samples. ^{1}H and ^{13}C NMR spectra were recorded at ambient temperature using Varian Unity Inova 600 and 400 MHz liquid state NMR spectrometers. Deuterated dimethyl sulfoxide (DMSO-d_6) and chloroform ($CDCl_3$) were used as solvents for sample dissolution. Positive-ion electrospray

ionization mass spectrometry (ESI-MS) was performed using a Waters Synapt G2 High-Resolution Mass Spectrometer to characterize the synthesized compounds.

Single crystal X-ray diffraction intensity data were collected on a Bruker DUO Apex II X-ray diffractometer equipped with an INCOATEC IμS HB microfocus tube (MoKα radiation λ = 0.71073) Å fitted with a multilayer monochromator. All structures were solved and refined using SHELX-2016 [11] employed within the X-Seed [12,13] environment.

All computations on the extractants (***L1-L5***) and their corresponding metal complexes were performed using Density Functional Theory (DFT) as implemented in the Gaussian 16 W software package. The calculations were conducted on the Lengau cluster at the Centre for High Performance Computing (CHPC) in Cape Town, South Africa. The DFT hybrid functional B3LYP (Becke-Lee-Yang-Parr) was chosen for its proven reliability in accurately describing exchange-correlation interactions. For the metal centres (Co, Ni, Mn), the LANL2DZ basis set [14–17] was employed, as it has been demonstrated to be suitable for describing the electronic properties of first-row transition metals. The 6–31 G (d, p) basis set was applied to describe the main elements (C, H, N, O) in the system.

2.3. Synthetic procedure

The most common method to make compounds of the amic acid type is a bimolecular nucleophilic substitution reaction. An amide bond is formed in the initial step of this synthesis through a coupling reaction with acyl chloride [18]. This bond is created by reacting acyl chloride with the desired primary amine.

To yield the new amic acid ligands, a bimolecular nucleophilic substitution (SN_2) reaction was used. Through a rigorous process in which the bond between the nucleophile and the carbon atom is formed concurrently with the cleavage of the bond between the carbon and the leaving group, this mechanism occurs when the nucleophile attacks the electrophilic carbon atom from the side opposite to the leaving group. A stereochemical inversion at the reaction centre is made possible by this combined mechanism. The Schotten-Baumann reaction is the approach used in this synthesis [19].

To achieve high-purity products, the crude materials were first subjected to solvent extraction technique by redissolving them in dichloromethane (DCM) and washing them with an acidic aqueous phase to effectively remove impurities. Further purification was carried out using either column chromatography or Kugelrohr distillation, depending on the nature of the compound.

2.3.1. Synthesis of glycine derivatives

2.3.1.1. Synthesis of N-Ethylglycine hydrochloride, GD1. 200 ml of dichloromethane (DCM) was added to a 250 mL round-bottom flask, and then monohydrate glyoxylic acid (7.60 g, 82.2 mmol) and ethylamine (1.90 g, 42.6 mmol) were added. At room temperature, the colourless mixture was stirred for about 24 h. A rotary evaporator was used to remove excess solvent (DCM), and a yellow solution was recovered as a crude product. The crude product was mixed with an aqueous solution of 1.0 M HCl (200 ml) and refluxed for 24 h. A yellow solid was produced after the solvent was removed and was recrystallized from MeOH/diethyl ether (1/5, V/V) ml. A yield of (3.42 g, 77.9 %), of white crystalline powder was recovered. FTIR-ATR (cm^{-1}) 3400 - 3300 (OH str), 3100 – 3000 (NH str), 2945 – 2726 (C—H str), 1740 (*C = O* str). ^{1}H NMR (400 MHz, DMSO-d_6) δ 1.20 (t, 3H, H1), 2.96 (q, 2H, H2), 3.31 (broad s, 1H, H3) 3.83 (s, 2H, H4), 9.03 (broad s, 1H, H6). δ Expected mass (g/mol): 103.06 ESI-MS (*m/z*) 104.07 $(M + H)^+$, 126.06 $(M+Na)^+$. m.p. (180 – 181) °C.

2.3.1.2. Synthesis of N-Isobutylglycine hydrochloride, GD2. Isobutylamine (3.20 g, 43.7 mmol) and monohydrate glyoxylic acid (12.1 g, 131 mmol) were used. The same process as outlined in *Section 3.3.1.1* was applied. The product yield (3.65 g, 63.7 %) was collected as a white, shimmering powder. FTIR-ATR (cm^{-1}) 3400 - 3300 (OH str), 3100 – 3000 (NH str), 2945 – 2726 (C—H str), 1740 (*C = O* str). ^{1}H NMR (400 MHz, DMSO-d_6) δ 0.92 – 0.93 (d, 6H, H1/3), 1.93 – 2.00 (m, 1H, H2), 2.87 – 2.88 (d, 2H, H4), 3.83 (s, 2H, H6). δ. Expected mass (g/mol): 131.09 ESI-MS (*m/z*) 132.10 $(M + H)^+$, 154.08 $(M+Na)^+$. m.p. (224 – 225) °C.

2.3.2. Synthesis of 2-chloroacetamide intermediates

2.3.2.1. Synthesis of 2-chloro-N, N-dioctylacetamide, CAI1. With a few slight adjustments, the following 2-chloroacetamide intermediates, *CAI1 and CAI2,* were synthesized using a method described in the published literature [6]. After charging a 200 ml round-bottom flask with 100 ml DCM, dioctylamine (24.1 g, 99.8 mmol) and triethylamine (10.1 g, 99.8 mmol) were added. Over a span of 45 min, 2-chloroacetyl chloride (13.6 g, 120 mmol) was added dropwise while the mixture was being stirred. After that, the reaction continued to stir for three more hours at room temperature. The reaction was allowed to cool at room temperature before being purified with a 0.1 M HCl solution, and then repeatedly washed with deionized water. After washing, anhydrous sodium sulphate was used to dry the organic layer.

The result was a dark orange solution with a yield of (28.6 g, 90.3 %). FTIR-ATR (cm^{-1}) 2954 - 2853 (CH str), 1643 (*C = O* str). ^{1}H NMR (600 MHz, $CDCl_3$) δ 0.87 (q, 6H, H1/16), 1.28 (m, 20H, H2/3/4/5/6/11/12/13/14/15), 1.93 – 1.96 (m, 4H, H8/9), 3.27 – 3.30 (m, 4H, H7/10), 4.05 (s, 2H, H18). Expected mass (g/mol): 317.3 ESI-MS (*m/z*) 318.3 $(M + H)^+$.

2.3.2.2. Synthesis of 2-chloro-N, N-dihexylaetamide, CAI2. For the synthesis of ***CAI2***, triethylamine (10.1 g, 99.8 mmol), dihexylamine (24.1 g, 100 mmol), and 2-chloroacetyl chloride (13.6 g, 120 mmol) were used, following the previously described method. A light-yellow oil was recovered as a product, yielding (21.3 g, 82 %). **FTIR-ATR** (cm^{-1}) 2954 - 2853 (CH str), 1643 (*C = O* str). **^{1}H NMR** (600 MHz, $CDCl_3$) δ 0.87 – 0.89 (m, 6H, H1/12), 1.29 – 1.31(m, 12H, H2/3/4/9/10/11), 1.55 – 1.59 (m, 4H, H5/8), 3.27 (t,2H, H6), 3.32 (t, 2H, H7), 4.05 (s, 2H, H14). **Expected mass** (g/mol): 261.2 **ESI-MS** (*m/z*) 262.2 $(M + H)^+$.

2.3.3. Synthesis of tridentate amic acid extractants

2.3.3.1. Synthesis of (2-(dioctylamino)-2-oxoethyl) glycine, L1. A 200 ml round-bottom flask was loaded with 100 ml of dry methanol, and at room temperature, (2.60 g, 65.0 mmol) of NaOH was dissolved in the alcohol. Glycine (4.90 g, 65.0 mmol) was added and after it had dissolved, the reaction mixture was stirred until a uniform milky solution was obtained. Over a span of 30 min, *CAI1* (4.20 g, 13.0 mmol) was added dropwise to the stirring solution. At 60 °C, the reaction mixture was stirred for 15 h. MeOH was extracted using a rotary evaporator to produce a crude product, which was then dissolved in DCM. The organic layer was purified by washing with 1.0 M H_2SO_4 and repeatedly with deionized water. After that, anhydrous sodium sulphate was used to dry the organic layer. The drying agent was then filtered off and the filtrate was concentrated via a rotary evaporator to remove excess solvent. A pure product was obtained as a yellow amorphous solid, (3.54 g, 76.4 %). FTIR-ATR (cm^{-1}) 3381(O—H), 3126 (N—H), 2953 –2851 (C—H str), 1648 – 1622 (*C = O* str). ^{1}H NMR (600 MHz, $CDCl_3$) δ 0.83 – 0.87 (m, 6H, H1/16), 1.23 (s, 20H, H2/3/4/5/6/11/12/13/14/15), 1.48 – 1.49 (m, 4H, H7/10), 3.09 – 3.13 (t, *J* = 11.5, Hz, 2H, H8), 3.23 – 3.26 (t, *J* = 9.2 Hz, 2H, H9), 3.58 (s, 2H,H18), 3.98 (s, 2H, H19), 7.83 (broad s, 1H, H21). ^{13}C NMR (600 MHz, $CDCl_3$) δ 14.03 (C1/16), 22.76 (C2/15), 26.84 (C11), 27.10 (C6), 27.53 (C10), 28.66 (C7), 29.17 (C12), 31.74 (C5), 46,27 (C19), 47.16 (C9), 50.15 (C8), 56.30 (C18), 164.87 (C17), 170.48 (C20). Expected mass ($g.mol^{-1}$) 356.30. ESI – MS (*m/z)* 357.31

$(M + H)^+$. m.p. (336 – 337) °C.

2.3.3.2. Synthesis of (2-(dioctylamino)-2-oxoethyl) methylglycine, L2. The previously described method in Section 3.3.3.1 was used for the synthesis of *L2*. NaOH as alkaline catalyst (4.80 g, 120 mmol), methylglycine (10.7 g, 120 mmol), *CAI1* (12.7 g, 40.0 mmol) were used. A pure product was obtained as a brownish-yellow amorphous solid, (10.1 g, 68.2 %). FTIR-ATR (cm^{-1}) 3381(O—H), 3126 (N—H), 2953 −2851 (C—H str), 1648 – 1622 (*C = O* str). ^{1}H NMR (600 MHz, $CDCl_3$) δ 0.84 – 0.86 (m, 6H, H1/16), 1.25 (s, 20H, H2/3/4/5/6/11/12/13/14/15), 1.49 – 1.50 (m, 4H, H7/10), 2.72 (s, 3H,H21), 3.12 – 3.14 (t, *J* = 12.1 Hz, 2H, H8), 3.25 – 3.27 (t, *J* = 11.8 Hz, 2H, H9), 3.53 (s, 2H,H18), 3.79 (s, 2H, H19), 7.86 (broad s, 1H,H22). ^{13}C NMR (600 MHz, $CDCl_3$) δ12.54 −14.06 (C1/16), 22.63 (C2/15), 26.87(C11),27.00(C6),27.56 (C7),28.81(C10),29.25(C4/5),31.73(C12/13),46.77(C3/14),47.06 (C21),50.36(C8/9),56.27(C18),58.20(C19),170.32(C17), 173.36(C20). Expected mass ($g.mol^{-1}$) 370.32. ESI – MS *(m/z)* 371.32 $(M + H)^+$. m.p. (327– 328) °C.

2.3.3.3. Synthesis of (2-(dioctylamino)-2-oxoethyl) ethylglycine, L3. The previously described method in *Section 3.3.3.1* was employed for the synthesis of *L3*. NaOH as alkaline catalyst (0.30 g, 8.2 mmol), ethylglycine (0.70 g, 6.8 mmol), *CAI1* (0.40 g, 1.4 mmol) were used. A pure product was obtained as a brownish - yellow amorphous solid, (0.35 g, 65 %). FTIR-ATR (cm^{-1}) 3415(O—H), 3094 (N—H), 2953 −2853 (C—H str), 1650 (*C = O* str). ^{1}H NMR (600 MHz, $CDCl_3$) δ 0.85 – 0.87 (m, 6H, H1/16), 1.11–1.14 (t, *J* = 9.8 Hz, 3H, H22), 1.52 (s, 20H, H2/3/4/5/6/11/12/13/14/15), 2.88 – 2.94 (q,2H,H21), 3.12 – 3.16 (t, *J* = 11.7 Hz, 2H, H8), 3.28 – 3.32 (t, *J* = 12.3 Hz, 2H, H9), 3.42 (s, 2H, H18), 3.67 (s, 2H, H19), 6.36 (broad s, 1H, H23). ^{13}C NMR (600 MHz, $CDCl_3$) δ 12.54 (C22),14.09(C2/15), 22.63(C2/15),26.87(C11),27.00(C6),27.56 (C7),28.81(C10),29.25,(C4/5),31.73(C12/13),46.77(C3/14),47.06 (C21),50.36(C8/9),56.27(C18),58.20(C19),170.32(C17),173.36(C20). Expected mass ($g.mol^{-1}$) 384.34. ESI – MS *m/z* 385.34 $(M + H)^+$. m.p. (338 – 339) °C.

2.3.3.4. Synthesis of (2-(dioctylamino)-2-oxoethyl)-N-isobutylglycine, L4. The synthesis of *L4* was carried out using the previously mentioned procedure in *Section 3.3.3.1*. *CAI1* (0.20 g, 0.63 mmol), isobutylglycine (0.40 g, 3.2 mmol), and NaOH (0.20 g, 3.8 mmol) was used as an alkaline catalyst. The product was a brownish-yellow oil (0.72 g, 55 %). FTIR-ATR (cm^{-1}) 3415.4(O—H), 3128(N—H), 2956.43–2853.33(C—H str), 1643.86(*C = O* str). ^{1}H NMR (600 MHz, $CDCl_3$) δ 0.85 – 0.87 (m, 12H, H1/16/24/25),1.28(s,20H, H2/3/4/5/6/11/12/13/14/15), 1.52 – 1.54 (m, 4H, H7/10), 1.65 – 1.72 (m,1H, H23), 2.40 – 2.51 (d, *J* = 11.6 Hz, 2H, H22), 3.11 – 3.15 (t, *J* = 12.2 Hz, 2H, H8), 3.29 – 3.34 (t, *J* = 11.9 Hz, 2H, H9), 3.37 (s, 2H, H18), 3.96 (s, 2H, H19). ^{13}C NMR (600 MHz, $CDCl_3$) δ 13.13(C1/16), 19.18(C24/25),21.59(C2/15),25.96 (C23),28.21(C6/11), 30.71(C4/5/7/10/12/13), 46.03(C3/15),56.43 (C8/9), 58.98(C18),63.65(C19), 170.48(C17), 172.87(C20). Expected mass ($g.mol^{-1}$) 412.37. ESI – MS *(m/z)* 413.37 $(M + H)^+$.

2.3.3.5. Synthesis of (2-(dihexylamino)-2-oxoethyl) methylglycine, L5. The previously described method in *Section 3.3.3.1* was employed for the synthesis of *L5*. NaOH as alkaline catalyst (0.20 g, 6.1 mmol), methylglycine (0.50 g, 6.1 mmol), *CAI2* (0.50 g, 2.0 mmol) were used. A pure product was obtained as a yellowish solid, (1.31 g, 68.2 %). FTIR-ATR (cm^{-1}) 3391 (O—H), 3100 (N—H), 2954 - 2854 (C—H str), 1625 (*C = O* str). ^{1}H NMR (600 MHz, $CDCl_3$) δ 0.83 – 0.85 (m, 6H, H1/12), 1.30 (m, 12H, H2/3/4/9/10/11), 1.53 – 1.55 (m,4H, H5/8), 2.89 (s, 3H, H15), 3.15 – 3.19 (t,*J* = 11.8 Hz 2H, H6), 3.28 – 3. 32 (t, *J* = 13.0 Hz, 3H, H7), 3.82 (s, 2H, H7), 4.20 (s, 2H, H16). ^{13}C NMR (600 MHz, $CDCl_3$) δ 13.97 (C1/12), 22.55(C2/11), 26.44(C3/10),26.70(C4/9),27.51(C5/8),28.71 (C15),31.47(C6/7), 56.58(C14),58.44(C16), 166.06(C13),170.26(C17). Expected mass ($g.mol^{-1}$) 314.26. ESI – MS *(m/z)* 313.35 $(M - H)^+$. m.p. (282 – 283) °C.

2.4. Description of the DFT method

All density functional theory (DFT) calculations for ligands **L1**–**L4** and their corresponding **L2** and **L3** copper(II) complexes were performed using the *Gaussian* (G16 C01) software package available on the Lengua cluster of the Centre for High-Performance Computing [CHPC, www.chpc.ac.za], Cape Town, South Africa [20]. The hybrid functional B3LYP was employed due to its proven reliability in modelling systems involving both organic ligands and transition metal centres [21]. Geometry optimizations were conducted in the gas phase at 298 K using the LANL2DZ basis set [22] with effective core potentials (ECPs) for transition metals (Co, Ni, Mn), and the 6–31G(d,p) basis set for main-group elements (C, H, N, O), providing a balanced compromise between computational cost and accuracy.

To verify the nature of the optimized structures as true energy minima, vibrational frequency analyses were performed to confirm the absence of imaginary frequencies. A thorough conformational analysis was undertaken to evaluate multiple stereoisomers and conformers, with the lowest energy structures discussed herein. Molecular visualization and input preparation were carried out using *GaussView 6.0.16*. Key geometric parameters, including bond lengths, angles, and dihedrals, were extracted and analysed to correlate with experimental crystallographic data and assess the structural effects of alkyl substituents on metal coordination behaviour.

3. Results and discussion

3.1. The three-step synthesis of tridentate amic acid ligands

The Schotten-Baumann reaction approach was adapted as a green synthesis method for amides due to its use of non-hazardous solvents. It was chosen as the best method for this study to acylate amino acids; this reaction is commonly employed for preparing various amic acid-type ligands with simple backbones, such as primary or secondary amines and acyl chlorides.

Step 1: The N – alkylation of amino acids

Step 2: Synthesis of acetamide precursors via a reaction of acyl chlorides with amines

Step 3: Synthesis of the novel amic acid ligand via a bimolecular nucleophilic substitution (SN_2) reaction (Scheme 1).

During the synthesis of these ligands, one of the things that was considered was the type of amine used. The reaction employed a significant excess of the primary amine (e.g., glycine) to suppress the formation of products where a single amino acid molecule reacts with two precursor molecules. Conversely, secondary amines (e.g., methylglycine) possess only one reactive site, eliminating the need for such an excess.

Various techniques were employed to confirm the identity and purity of the products, as well as to assess their physicochemical properties relevant to their application as metal extractants. To investigate the characterization process, a single representative from the three-step synthesis (N-formyl glycine derivative, 2-chloro-N, N-acetamide, and amic acid extractant) will be selected for a detailed analysis. All other characterization data will be in the supplementary information.

From the FTIR spectrum (Fig. 2*)* of N-Ethylglycine, we observed a broad signal around 3394 cm^{-1}. This indicates the presence of an OH (hydroxyl) group in the molecule. There is also a sharper peak at 3167 cm^{-1}, which confirms that N-Ethylglycine is a secondary amine group.

The NMR analysis supports the successful synthesis of N-Ethylglycine. Specific peaks help to show the different parts of the molecule. As illustrated in Fig. 3, a triplet around 1.3 ppm corresponds to the three protons in the methyl (CH_3) group. A quartet of around 3.3 ppm signifies the two hydrogens in the methylene (CH_2) group between the amine (NH) and CH_3 group. Finally, a single peak at 3.9 ppm indicates the two

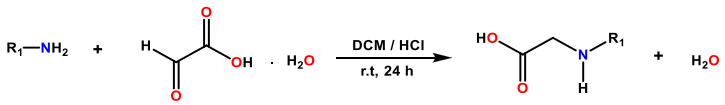

Step 1: The N – alkylation of amino acids

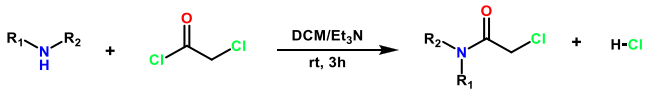

Step 2: Synthesis of acetamide precursors via a reaction of acyl chlorides with amines

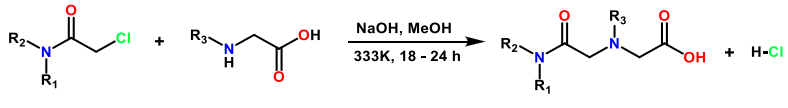

Step 3: Synthesis of the novel amic acid ligand via a bimolecular nucleophilic substitution (SN_2) reaction

Scheme 1. Reaction scheme 1: General synthesis of tridentate amic acid extractants.

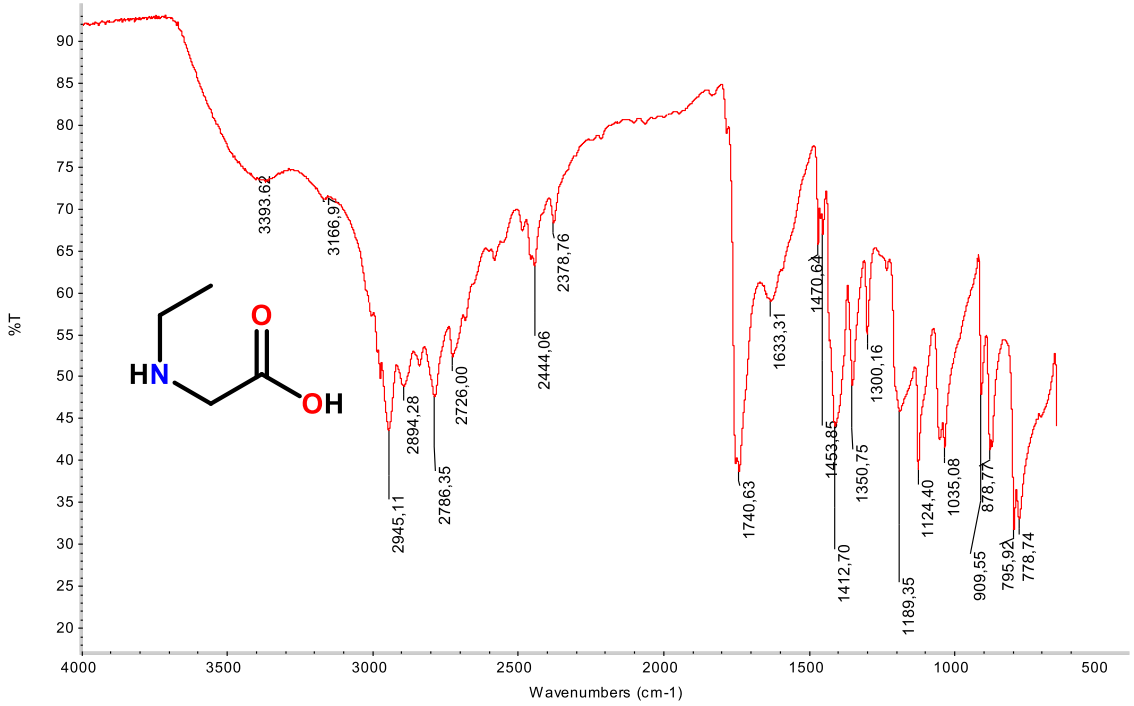

Fig. 2. FTIR-ATR spectrum for N-Ethylglycine, GD1.

hydrogens in the CH_2 group located between the amine (NH) and the carboxylic acid group (COOH). Since N-Ethylglycine is a well-established compound, further characterization techniques were not necessary.

The OH and NH protons generally exhibit broad singlets in ^1H NMR spectra due to rapid exchange processes with solvent protons. This exchange broadening obscures any potential coupling interactions with neighbouring protons. However, when D_2O is used as the solvent, the exchangeable OH and NH protons are replaced with deuterium atoms, forming OD and ND groups, respectively.

These deuterated species are not detectable by standard ^1H NMR spectroscopy, as they do not have a large ^1H NMR signal. Hence these signals are not visible on the spectrum obtained for ***GD1***.

Prior to the synthesis of the target ligand, the successful formation of the 2-chloro-N, N-acetamide precursor was verified using FTIR-ATR and NMR techniques. Analysis of the FTIR spectrum (Fig. 4(a)) revealed a sharp absorption band at approximately 1645 cm^{-1}, which is characteristic of the amide carbonyl ($C = O$) functionality, confirming its successful formation.

Furthermore, ^1H NMR spectroscopy was used to ensure the purity of the precursor before proceeding with the final synthesis step to produce the desired aminocarbonylmethyl amino acid extractant. As depicted in

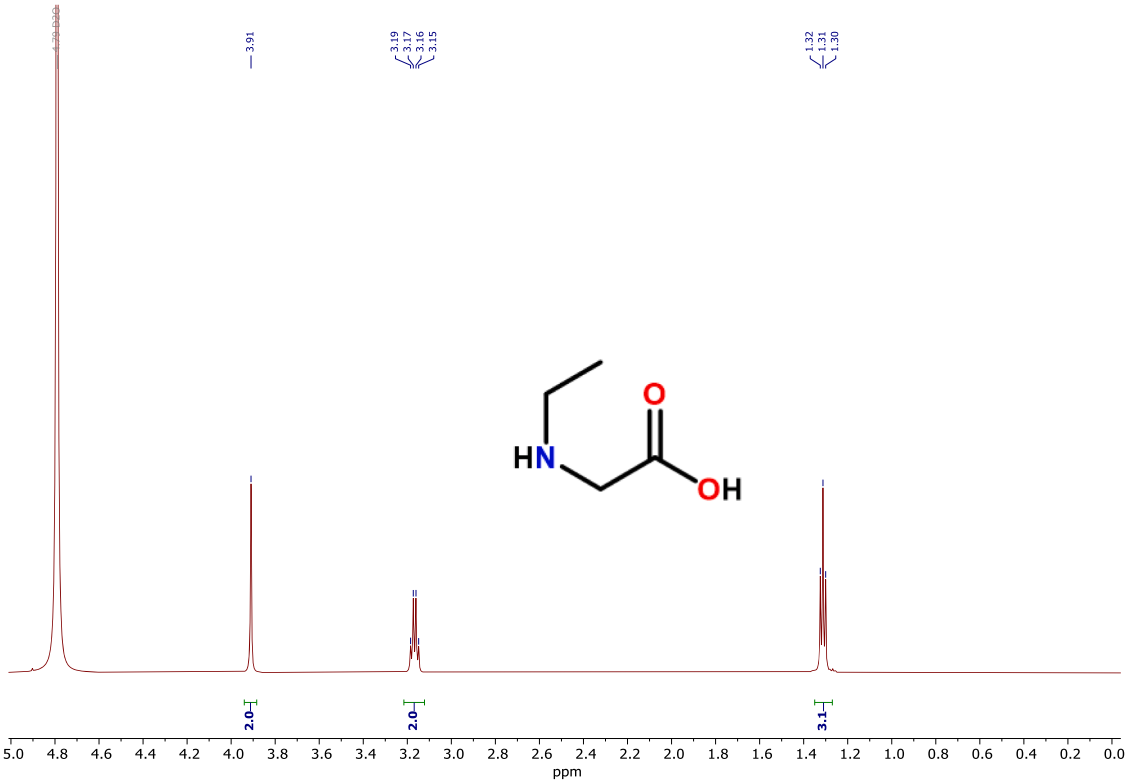

Fig. 3. ^{1}H NMR spectrum for N-Ethylglycine, GD1.

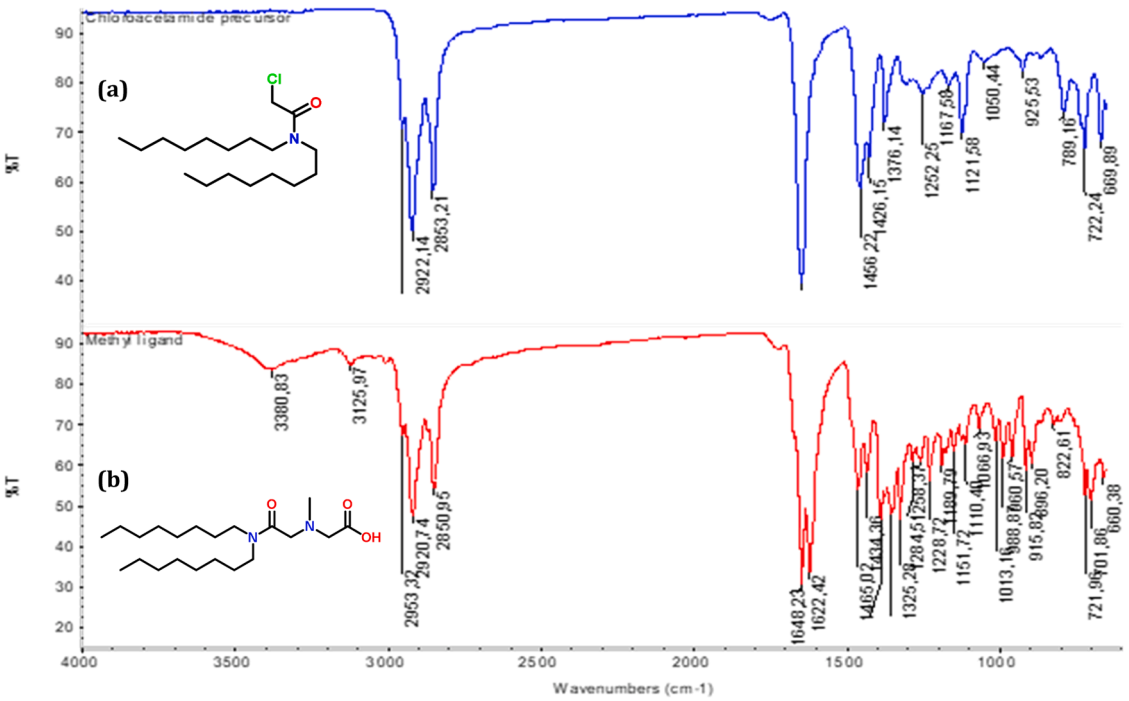

Fig. 4. Stacked FTIR-ATR spectrum for (a) 2-chloro-N, N-dioctylacetamide and (b) N-(2-(dioctylamino)-2-oxoethyl)-N-methylglycine.

Fig. 5, a distinct peak at 4.05 ppm was assigned to the methylene (CH_2) protons situated between the chlorine atom (Cl) and the amide group. Additionally, the presence of signals within the aliphatic region (0.87 – 1.28 ppm) confirmed the presence of the expected alkyl chain methyl (CH_3) and methylene (CH_2) protons.

FTIR-ATR spectroscopy was employed to monitor the formation of the amic acid ligand. The appearance of a broad absorption band at approximately 3380 cm^{-1} in the spectrum (Fig. 4(b)) signifies the presence of the OH functionality associated with the carboxylic acid group of the amino acid component.

Furthermore, the spectrum revealed a slight shift of the amide carbonyl peak to 1648 cm^{-1} compared to the precursor (Fig. 4(a)). This

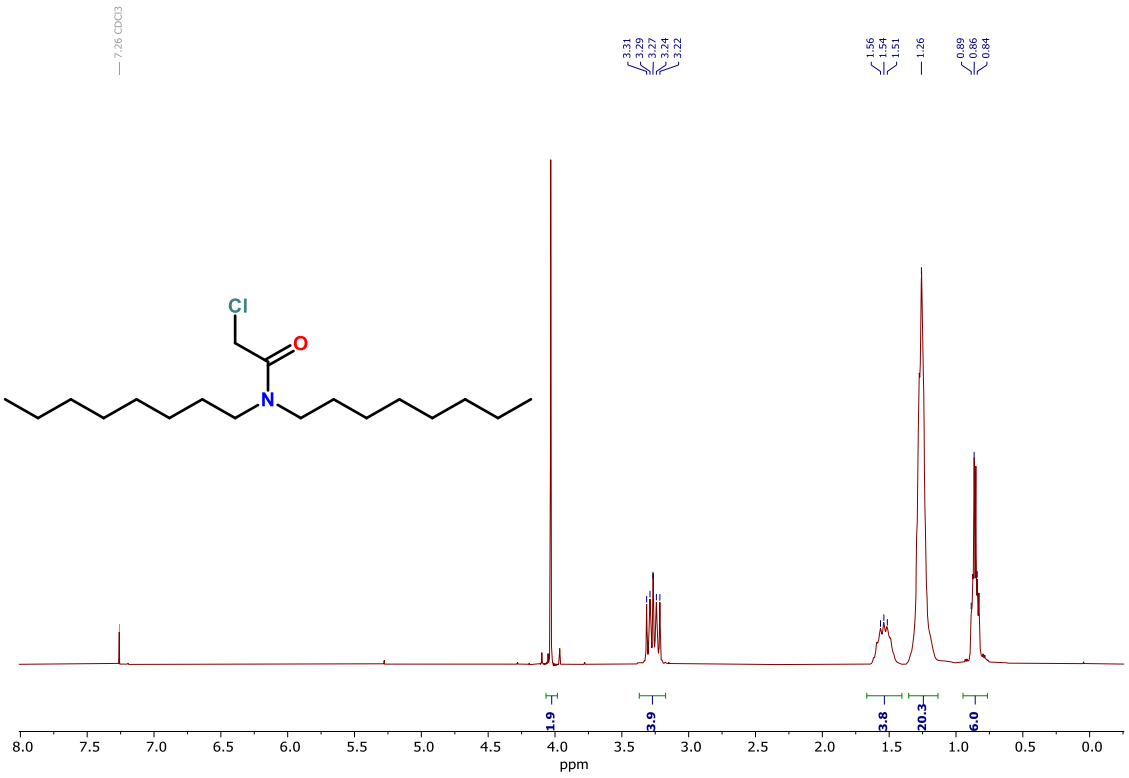

Fig. 5. ^{1}H NMR spectrum for 2-chloro-N, N-dioctylacetamide, CAI1.

confirms the successful formation of the amino acid moiety. An additional characteristic peak appeared at around 1622 cm^{-1}, which can be attributed to the carboxylic carbonyl group of the newly formed amic acid.

^{1}H- and ^{13}C NMR spectroscopy provided further compelling evidence for the successful synthesis of the target amic acid extractants. Compared to the spectrum of the precursor, 2-chloro-N, N-acetamide, the disappearance of the characteristic peak at approximately 4.2 ppm in the ^{1}H NMR spectrum (Fig. 6) confirms the leaving of the chlorine atom (good leaving group). This observation signifies the formation of a new bond between the amino acid moiety and the amide carbonyl carbon. A new peak at around 3.9 ppm is attributed to the methylene (CH_2) protons situated at this newly formed linkage.

The ^{1}H NMR spectrum also revealed the presence of a proton within the composite carboxylic acid group at about 7.9 ppm. However, it is important to note that this peak may not be visible for all amic acid extractants due to the previously explained phenomenon of hydroxyl (OH) exchangeable protons. This exchange process averages out the chemical environment of the OH proton, leading to the broadening and potential disappearance of its signal into the baseline noise of the spectrum.

As illustrated in Fig. 7, the ^{13}C NMR spectrum of ***L2*** displayed well-resolved signals, facilitating straightforward assignment of the peaks to the corresponding carbon atoms in the molecular structure. The two downfield resonance peaks observed at 170.3 and 173.6 ppm in the ^{13}C NMR spectrum were assigned to the carbonyl carbons of the amide and carboxylic acid groups, respectively. The difference in chemical shift between these two carbonyl carbons can be attributed to the difference in electronegativity of the neighbouring atoms. The nitrogen atom, being less electronegative than the oxygen atom, exerts a weaker electron-withdrawing effect on the adjacent carbonyl carbon, resulting in a less downfield chemical shift for the amide carbonyl carbon compared to the carboxylic acid carbonyl carbon.

The alkyl CH_2 carbon atoms, which are influenced by the electron-

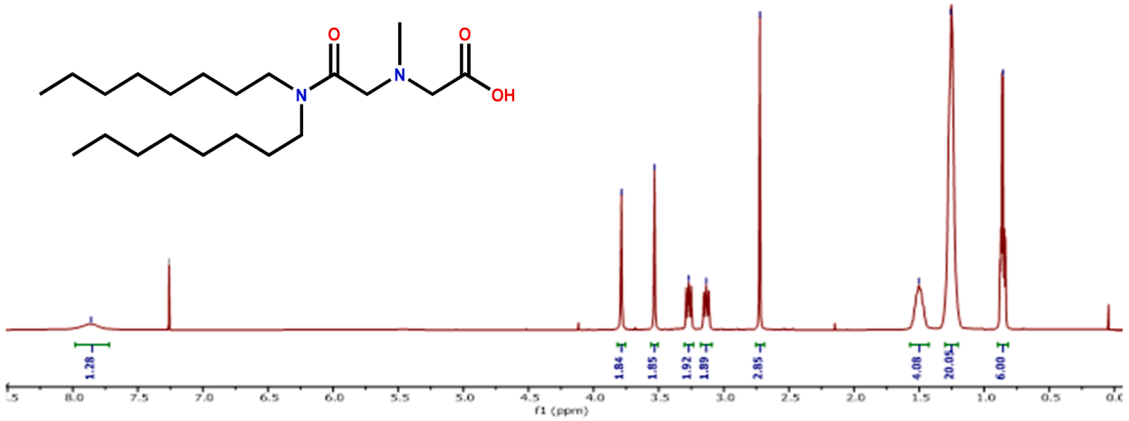

Fig. 6. ^{1}H NMR spectrum for N-(2-(dioctylamino)-2-oxoethyl)-N-methylglycine, L2.

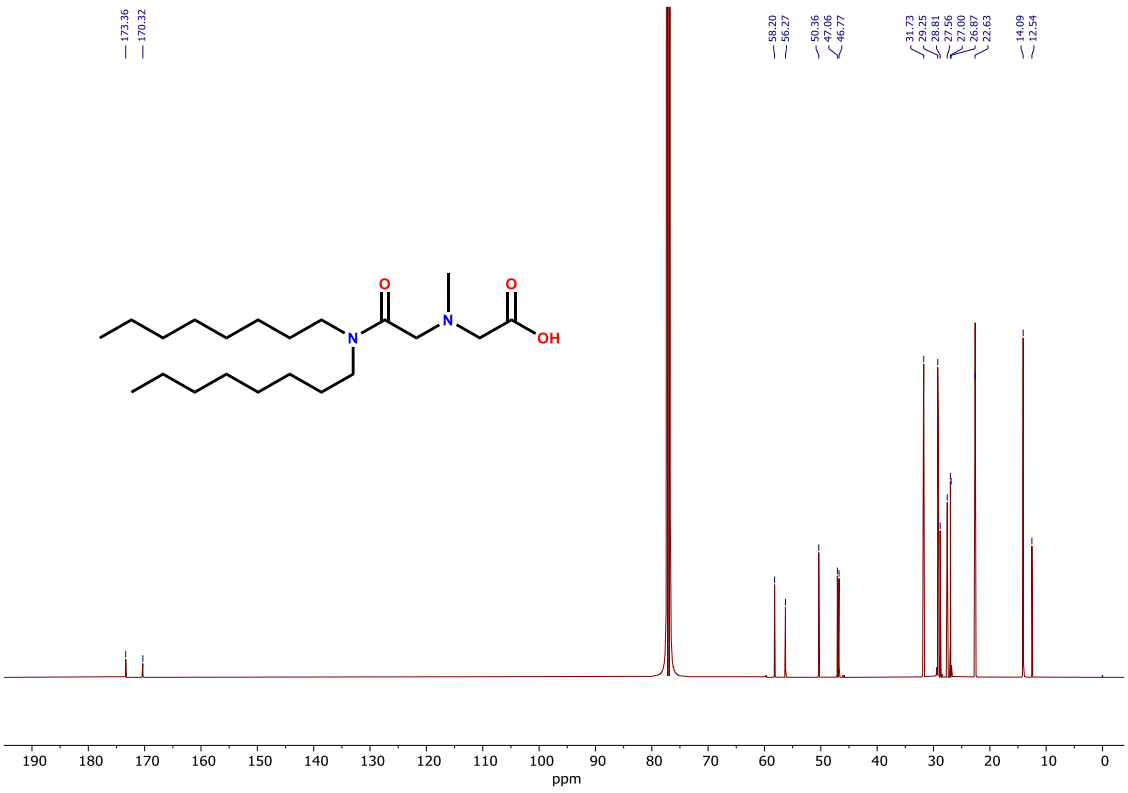

Fig. 7. ^{13}C NMR spectrum for N-(2-(dioctylamino)-2-oxoethyl)-N-methylglycine, L2.

withdrawing effect of the amide nitrogen atom, showed distinct chemical shifts at 14.09, 22.63, 27.56, and 28.81 ppm. The differences in chemical shift can be attributed to the varying degrees of electron density at these carbon atoms, which are influenced by their proximity to the electron-withdrawing amide group. The NCO—CH_2-N and -N-CH_2-COOH carbons were assigned to 56.27 and 58.20 ppm, respectively. The methyl carbon atom, which is directly attached to a nitrogen atom, showed a chemical shift of 46.7 ppm.

The successful synthesis of ***L2*** was confirmed by mass spectrometry (MS) and elemental analysis, which yielded results consistent with the expected molecular formula. For a more comprehensive analysis of the synthesized compounds, including glycine derivatives, acetamide intermediates, and amic acid ligands, please refer to the supplementary information.

3.2. *Crystallographic studies*

The challenge in growing crystals for these amic acid ligands was caused by the presence of extended *n*-alkyl arms, which can result in inefficient packing and considerable disorder. Nevertheless, competitive extraction studies including Cu^{2+}, ***L2*** and ***L5*** demonstrated high extraction efficiencies This implies that the organic loaded phase exhibited significantly higher Cu concentrations in comparison to other base metal ions. Considering the chemical bonding properties of Cu^{2+}, it has a smaller ionic radius (0.57 Å), thus its strong affinity for these extractants was anticipated. This proposes that the Cu^{2+} extracted complexes were the most stable species in the organic phase, making them more susceptible to undergo crystallization.

To facilitate crystal growth, single extraction experiments were performed under optimal conditions using a relatively high-volume ratio of 1:1 (5 mL: 5 mL; O/A). This was to ensure sufficient organic loaded phase for subsequent crystal growth. To accelerate the formation of a supersaturated solution and reduce the overall crystallization time, the organic-loaded phase was concentrated using a rotary evaporator, reducing the volume from 4 to 2 mL. The supersaturated solution was then allowed to evaporate slowly at room temperature, promoting crystal growth.

Single crystals of **Cu(L2)$_2$** and ***Cu(L5)$_2$***., proper for X-ray diffraction analysis, were grown by the slow evaporation of chloroform as a solvent, see Fig. 8(a) *and* ***(b)***. This technique involves the steady evaporation of the solvent, leading to the formation of well-defined single crystals suitable for structural characterization. Summarized crystallography data as well as structural parameters are presented in Table 1 while the molecular structures of the complexes were drawn by exploring mercury software [23].

Both **Cu(L2)$_2$** and **Cu(L5)$_2$** crystallize as monoclinic, with a space group of $P2_1/c$ and $C2/c$ for **Cu(L2)$_2$** and **Cu(L5)$_2$** respectively. The asymmetric units of **Cu(L2)$_2$** and **Cu(L5)$_2$** contain half of a molecule and solvents such as chloroform and a water molecule in **Cu(L2)$_2$** and **Cu (L5)$_2$** respectively.

To the best of our knowledge, no earlier studies have reported the fundamental coordination chemistry through crystal structures of amic acid-type ligands with base metal ions. A thorough search of the Cambridge Structural Database (November 2024 update) revealed no closely related structures to the Cu complexes or the ligands reported in this study. This suggests this work is the first report of Cu crystal structures for amic acid-based extractants. Hence this research represents a significant step forward, bridging the gap between solution-based extraction and solid-state analysis.

In solvent extraction, the formation of the most stable metal complexes is preferentially favoured. The strength of the metal-ligand bond is a key factor influencing complex stability, which influences extraction performance. Therefore, it was of interest to investigate the bond length between; M – N, M – O_{amide}, and M – $O_{carboxylic}$. For a detailed comparison of the important bond lengths and angles within the **Cu(L2)$_2$** *and* **Cu(L5)$_2$** complexes, please refer to Table 2. Shorter bond lengths are indicative of stronger coordination interactions [24].

Comparing the metal-ligand bonds Cu1-O1, M–$O_{carboxylic}$ were shorter for each Cu^{2+} complex;(1.938 and 1.986) Á, **Cu(L2)$_2$** *and* **Cu (L5)$_2$** respectively. This reflects a strong interaction between the

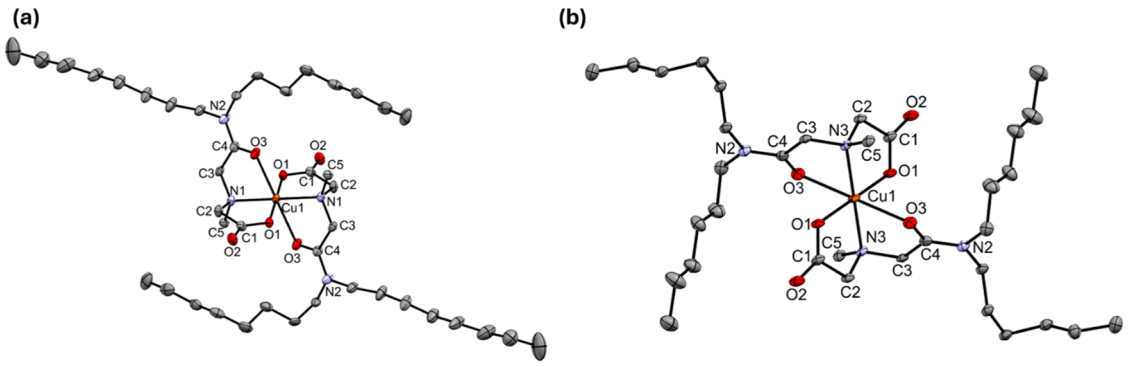

Fig. 8. Crystal structure for complex **(a) Cu(L2)$_2$** and **(b) Cu(L5)$_2$** drawn at 50 % thermal ellipsoids probability. Disordered chloroform solvent and hydrogen atoms have been omitted for clarity.

Table 1
X-ray crystallographic data collection and refinement parameters for **Cu(L2)$_2$**, and **Cu(L5)$_2$** complexes.

Compound	*Cu(L2)$_2$*	*Cu(L5)$_2$*
Empirical formula	$C_{44}H_{84}Cl_6CuN_4O_6$	$C_{34}H_{70}CuN_4O_8$
Formula weight	1041.39	726.48
Temperature/K	100(2)	100(2)
Crystal system	monoclinic	monoclinic
Space group	$P2_1/c$	$C2/c$
a/Å	6.8732(6)	28.069(7)
b/Å	20.252(2)	15.304(4)
c/Å	19.916(2)	9.475(2)
α/°	90	90
β/°	99.398(3)	99.965(5)
γ/°	90	90
Volume/Å^3	2735.0(5)	4008.9(18)
Z	2	4
ρ_{calc}g/cm^3	1.265	1.204
μ/mm^{-1}	0.737	0.594
F(000)	1110	1580
Crystal size/mm^3	0.301 'x 0.112 x' 0.036	0.126 × 0.086 × 0.037
2Θ range for data collection/°	2.011 to 25.408	1.473 to 25.721
Index ranges	$-8 \le h \le 8$ $-24 \le k \le 24$ $-23 \le l \le 23$	$-34 \le h \le 34$ $-18 \le k \le 18$ $-11 \le l \le 11$
Reflections collected	57,864	34,662
Independent reflections	5023 [R_{int} = 0.1293]	3816 [R_{int} = 0.1146]
Data/restraints/ parameters	5023 / 30 / 392	3816 / 0 / 225
Goodness-of-fit on F^2	1.032	1.044
Final R indexes [$I \ge 2\sigma$ (I)]	$R1$ = 0.0725, $wR2$ = 0.1558	$R1$ = 0.0584, $wR2$ = 0.1339
Final R indexes [all data]	$R1$ = 0.1076, $wR2$ = 0.1815	$R1$ = 0.0941, $wR2$ = 0.1513
Largest diff. peak/hole / e Å^{-3}	0.930 and −0.580	0.857 and −0.573

Table 2
Selected bond length and angles for complexes **Cu(L2)$_2$** and **Cu(L5)$_2$**.

	Cu(L2)$_2$	Cu(L5)$_2$
Bond distances (Å)		
Cu—O(3)	2.424	2.380
Cu—O(1)	1.938	1.986
Cu—N(1/3)	2.027	2.024
C4—N(2)	1.338	1.342
C4—C(3)	1.525	1.510
C4—O(3)	1.237	1.245
Bond angles (°)		
O(3) - Cu(1) - N(1/3)	72.97	71.10
N(1/3) - Cu(1) - O(1)	85.96	83.86
O(1) - Cu(1) - O(3)	86.15	83.52
O(3) - Cu(1) - N(1/3)	72.97	71.10
N(1/3) - Cu(1) - O(1)	85.96	83.86
O(3) - Cu(1) - O(1)	86.15	83.52

negatively charged oxygen donor (-OH) of the carboxylic acid group and the positively charged Cu metal ions. Additionally, **Cu(L2)$_2$** has a shorter C4-N2 bond, 1.338 Á, although the amide nitrogen does not participate directly in the formation of the Cu^{2+} complex, due to its low basicity from electron delocalization, it indirectly contributes to complex stability. C—N_{amide} increases electron density on the amide oxygen, M-O_{amide} owing to its partial C—N double bond character which enhances its basicity [25]. This primes to stronger electrostatic interactions with the metal ion, ultimately favouring stronger coordination.

Based on the structural similarities between ***L2*** and ***L5***, it was imagined that their respective Cu^{2+} complexes, **Cu(L2)$_2$** and **Cu(L5)$_2$**, would reveal the closest parameters. However, a detailed analysis of the copper-nitrogen bond (Cu1-N1/3) lengths showed a slight decrease in bond length for **Cu(L5)$_2$** compared to ***Cu(L2)$_2$***. Nevertheless, this difference was not significant.

The C4-N2 bonds in the Cu^{2+} crystal structures, **Cu(L2)$_2$** *and* **Cu(L5)$_2$** exhibited bond lengths ranging from (1.338 −1.342) Å. These bonds are relatively shorter than the typical C—N bond lengths in tertiary amides, suggesting a partial double bond character within the coordinating tridentate extractants. Due to the resonance stabilization within the amide bond moiety, the carbonyl bond may exist as a single bond in nature, consequently providing the C—N bond with a partial double bond character [26,27]. This indicates strong coordination between the amide group, the O-donor atoms and Cu1, which in turn results in larger bond angles compared to the idealized bond angles of a five-membered(1, 2-ethanediol) chelate ring [28].

Both complexes are mononuclear species with the Cu^{2+} centre coordinated to four oxygen atoms as well as two nitrogen atoms from two amic acid ligands, in a tridentate fashion as shown in Fig. 8. In this mode, four five-membered C_2NOCu chelate rings are formed with bite angles ranging from (71.10– 86.15) ° (Table 2). The values for the bite angles for all the complexes are smaller than the ideal 90° for a perfect octahedron, hence adopting distorted octahedral geometry [29]. However, when the structures are analysed with Mercury software, a very slight deviation from Oh geometry is seen as the angles are close and none of them were 100° which could cause a huge distortion.

At the metal centre, the basal plane consists of two nitrogen atoms from the tertiary nitrogen and one oxygen atom each from the amide and carboxylic functional group respectively while the remaining two oxygen atoms occupy the axial position of the octahedron.

For both complexes, each ligand formed two five-membered C_2NOCu chelate rings with the Cu^{2+} centre, with their plane almost perpendicular to each other (83.10° for ***Cu(L2)$_2$***), having a chair-like structure which is inverse to other coordinating ligands. It was observed that the equatorial Cu1–O1 distances are shorter than the one for axial Cu1–O3 i.e., in **Cu(L2)$_2$**, Cu1–O1 = 1.938 Á while Cu1–O3 = 2.424 Á, and this could be attributed to the Jahn-Teller effect [30]. The bond distances as

well as the bond angles are comparable to similar structures reported in the literature [16,31]. Another important feature in both structures is the trans arrangement of the nitrogen atoms of the ligands. This trans relationship between these donor atoms contributes to the overall stability of the complexes as the trans configuration minimizes steric interactions [32].

Furthermore, the carboxylic O atoms and carbonyl O atoms adopt a trans configuration as well, which further contributes to the overall geometry and stability of the complexes. As highlighted by Martell et al. [28,33], the bond length between a metal ion and a donor atom significantly changes the bond angle within the chelate ring. This, in turn, influences the overall stability and selectivity of the metal complex in extraction processes. This concept is analogous to the low-strain conformation of six(1,3-diaminopropane) and five(ethylenediamine)-membered chelate rings.

The angle formed between the two donor atoms (oxygen and nitrogen) and the metal centre in a coordinating complex, represented as O – Cu – N, is known as the bite angle. In the late 19th century, Dierkes *et al.* [34] studied the basic principles of the bite angle effect. They discovered that the ligand bite angle plays a major role in the rates and selectivity of catalytic processes.

Given the significant role of the geometric properties of a bite angle in determining selectivity, the crystal structures of Cu^{2+} complexes were studied to gain deeper insights into the selective extraction of Cu^{2+} ions compared to other base metal ions. This competitive extraction analysis will be fully discussed in a subsequent solvent extraction (SX) paper. The SX paper will mainly provide valuable information on the factors influencing selectivity towards Cu^{2+} metal ions. In coordination chemistry, when the bite angle is smaller, it characteristically restricts the three-dimensional arrangement around the metal centre, resulting in a smaller cavity size [34]. Cavity size is the space within the extractant structure that accommodates the metal ion.

3.3. Effect of steric and inductive effects on the coordination chemistry of N-donor ligands

The understanding of steric and inductive effects is important for the realistic design of N-donor ligands. By carefully considering the size and electronic properties of substituents, chemists can tailor the ligand structure to achieve specific coordination geometries and binding affinities, enabling the selective extraction of desired metal ions [35,36].

The chemistry between inductive effects and steric effects can be complicated; however, the donor strength has been established to increase in the following order: $NH_3 < NH_2CH_3 < NH\ (CH_3)_2 < NH(CH_3)_3$. While this order of substitution results in an increase in the electron-donating ability of the ligands, it also introduces steric bulk, which can hinder the coordination of metal ions [35,37]. Hence, in some cases, the steric effects of substituents can hinder the coordination of metal ions, even if the substituents have strong electron-donating properties [38]. It is well-established in the literature that N-alkylation often leads to a decrease in complex stability due to increased steric hindrance. However, N-methylation, with its relatively small methyl group, introduces minimal steric hindrance [38,39]. As a result, the inductive effect of the methyl group, which donates electron density to the nitrogen atom, becomes the dominant factor. This increased electron density on the nitrogen atom enhances its basicity, leading to stronger metal-ligand interactions [38].

Density Functional Theory (DFT) calculations were of interest to gain deeper insight into the influence of the *n*-alkyl substituents on the amine nitrogen (R^3 group) on the electronic structures of the compounds presented in this study.

3.4. Computational analysis: DFT studies

Hanada et al. [3] reported DFT calculations of the amic acid extractants that revealed high performance in separating Ni and Co from LiBs. From their study, they predicted that aliphatic substituents performed better than aromatic substituents. Given the potential impact of the *n*-alkyl substituent on the tertiary nitrogen atom of the amino acid group on extraction performance, ***L1, L3***, and ***L4***, representing structurally modified extractants, were included in this computational study. This computational approach aimed to explain the fundamental factors governing their extraction behaviour and selectivity for specific metal ions.

As outlined in Table 3, the positive inductive effect of the *n*-alkyl substituents, which are electron-donating groups, primarily influences the N2-C21 bond length linking the neutral nitrogen donor atom. Interestingly, the N2-C21 bond length did not increase further with the *n*-isobutyl substituent [40] (***L4***), suggesting that steric effects may rule over inductive effects in this case. Additionally, minimal to no changes were observed in the C4-O3 and C1-O1 bond lengths. This indicates that the electrostatic attraction of the negatively charged oxygen donor atoms is stronger, mitigating the impact of inductive effects on the C4-O3 bond. The rigid amide bond (C1-O1), stabilized by resonance, remains largely unaffected by the positive inductive effects. This argument affords a justification for the superior extraction performance of ***L2*** compared to ***L3*** and ***L4***.

Fig. 9 illustrates the minimum energy conformers of the amic acid extractants obtained by the DFT calculations. To better visualize the donor atoms that coordinate with the base metal ions during extraction, hydrogen atoms were removed, and *n*-alkyl chains were replaced by methyl groups. The structures were modified using GaussView post-optimization. However, this process did not change the reported bond lengths and angles.

A computational validation of X-ray crystallographic data of **$Cu(L2)_2$** and **$Cu(L3)_2$** was performed. A detailed comparison of the DFT-calculated bond lengths and angles for the copper complexes showed a significant degree of agreement with the crystallographic data from the experimental work, see Table 4. These findings suggest that the DFT calculations provide a reliable description of the electronic structure and geometry of the complexes.

The DFT-calculated and the reported X-ray crystallographic data for both **$Cu(L2)_2$** and **$Cu(L3)_2$** complexes are in good agreement.

However, it is noteworthy that the *n*-alkyl substituent on the N atom appears to exert an influence on the Cu-N(1) and N1-C(5) bonds while other bonds within the coordination sphere are somewhat not affected by the presence of the *n*-alkyl substituent. This observation highlights the key role of *n*-alkyl substitution on the nitrogen atom in influencing the electronic and steric properties of the extractant, which, in turn, affects the stability of the metal-ligand complexes. These refined changes in extractant structure can have a significant impact on the extraction efficiency. Figs. 10 and 11 illustrate the optimized low-energy structures for **$Cu(L2)_2$** and **$Cu(L3)_2$** complexes, respectively.

4. Conclusions

The design, synthesis, and comprehensive characterization of a new class of amic acid-based compounds, was achieved by strategically modifying the amino acid moiety and varying the *n*-alkyl chain length on the amide nitrogen. These compounds were synthesized via a straightforward SN_2 reaction between 2-chloroacetamide intermediates and a range of amino acids. Structural elucidation through a combination of spectroscopic techniques—^{1}H NMR, ^{13}C NMR, FT-IR

Table 3
Selected bond lengths of the donor atoms (Å) from optimal extractant structures.

	L1	*L2*	*L3*	*L4*
C4—O(3)	1.353	1.359	1.359	1.359
C1—O(1)	1.231	1.231	1.231	1.231
N2—C(21)	—	1.463	1.473	1.473
N2—H(3)	1.020	—	—	—

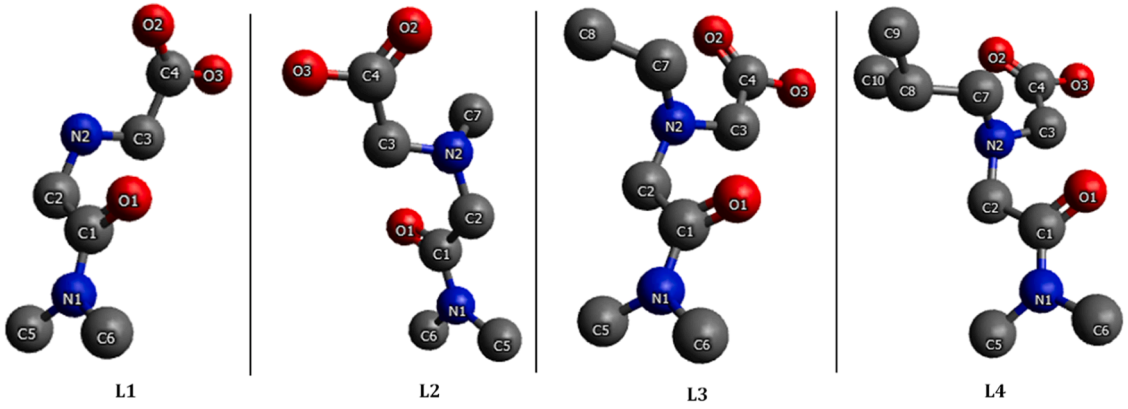

Fig. 9. Optimized extractant structures with different amino acid groups. Hydrogen atoms and the octyl-chains were removed for clarity.

Table 4
Selected bond length and angles for optimized complexes **Cu(L2)$_2$** and **Cu(L3)$_2$**.

	Cu(L2)$_2$	*Cu(L3)$_2$*
Bond distances (Å)		
Cu—O(3)	2.578	2.549
Cu —O(1)	2.003	2.000
Cu —N(1)	2.088	2.102
C2—N(1)	1.482	1.482
O3—C(4)	1.243	1.243
C3—C(4)	1.538	1.538
N1—C(5)	1.483	1.500
Bond angles (°)		
N(1) - Cu - O(5)	82.07	81.75
O(3) - Cu - O(1)	79.90	81.27
O(3) - Cu - N(1)	70.39	71.24
N(1) - Cu - O(1)	82.36	82.21
O(1) - Cu - O(3)	81.75	82.51
O(3) - Cu - N(1)	82.36	79.44

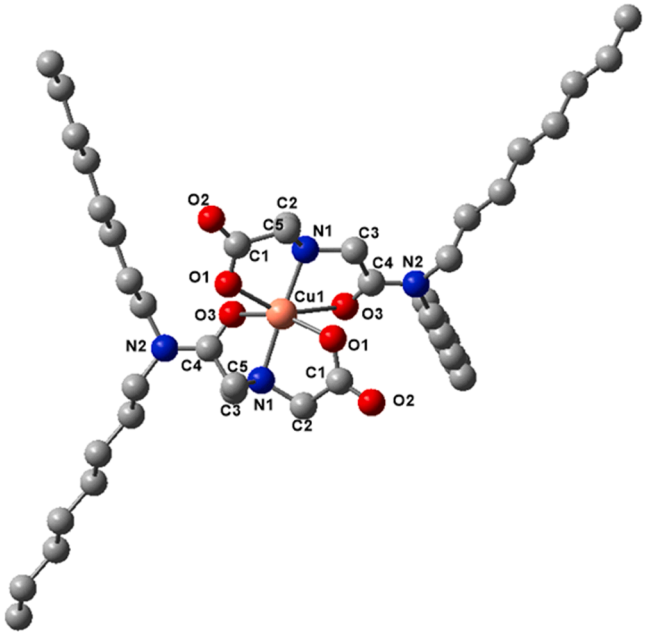

Fig. 10. Minimum energy conformer for Cu(L2)$_2$ complex. Hydrogen atoms have been removed for clarity.

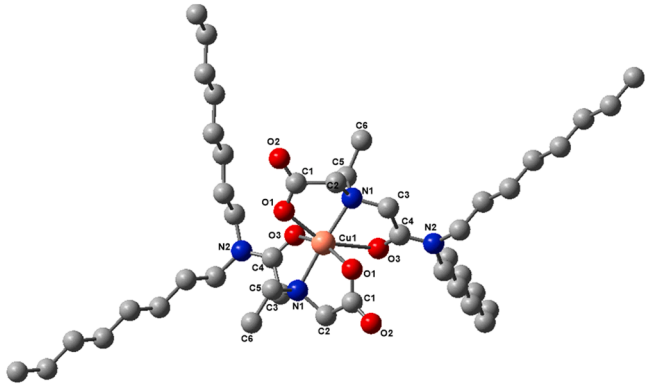

Fig. 11. Minimum energy conformer for Cu(L3)$_2$ complex. Hydrogen atoms have been removed for clarity.

spectroscopy, supported by mass spectrometry, and melting point data, confirmed the successful synthesis of these novel compounds.

To extend our understanding of these ligands, we adopted a multi-disciplinary approach that integrates solid-state analysis, solution-phase studies, and computational modelling. Notably, X-ray crystallographic studies of two copper(II) complexes, ***Cu(L2)$_2$*** and ***Cu(L5)$_2$*** provided the first reported crystal structures of amic acid-based metal complexes. These structures confirmed the tridentate coordination mode of the ligands and revealed detailed insights into the geometry around the metal centre, including key bond lengths and angles.

Complementary DFT calculations were employed to investigate how the nature of the *n*-alkyl substituents affects the electronic structure and stability of the complexes. The excellent agreement between the computational (DFT) and experimental (X-ray crystallographic) data for ***Cu(L2)$_2$*** and ***Cu(L5)$_2$*** validates the use of computational chemistry as a powerful predictive tool in transition metal coordination studies. These findings underscore the significant potential of combining experimental and theoretical methods to design and understand novel metal-binding ligands with relevance in extraction chemistry and beyond.

Supplementary information

CCDC 2454113 and CCDC 2454114 contain supplementary crystallographic data for compounds **Cu(L5)$_2$** and ***Cu(L2)$_2$***. These data can be obtained free of charge with the links 2454,113 (https://www.ccdc.cam.ac.uk/structures/search?Ccdcid=2454113&DatabaseToSearch=CSD) for ***Cu(L5)$_2$*** and 2454,114 (https://www.ccdc.cam.ac.uk/structures/search?Ccdcid=2448557&DatabaseToSearch=CSD) for ***Cu(L2)$_2$*** or from the Cambridge Crystallographic Data Centre, 12 Union Road, Cambridge CB2 1EZ, U.K.; fax: (+44)1223–336–033; or via e-mail:

deposit@ccdc.cam.ac.uk. Other supplementary information is attached.

CRediT authorship contribution statement

Nonkosi Matinise: Writing – review & editing, Writing – original draft, Validation, Methodology, Investigation, Formal analysis, Data curation. **Claire Ineza:** Validation, Methodology, Formal analysis, Data curation. **Segun D. Oladipo:** Writing – review & editing, Validation, Methodology, Investigation, Formal analysis, Data curation. **Nusrat M. Begum:** Validation, Methodology, Investigation, Formal analysis, Data curation. **Abosede A. Badeji:** Validation, Software, Resources, Investigation, Formal analysis. **Anton S. Lopis:** Validation, Software, Resources, Methodology, Investigation, Formal analysis, Data curation. **Robert C. Luckay:** Writing – review & editing, Supervision, Resources, Project administration, Funding acquisition, Formal analysis, Conceptualization.

Declaration of competing interest

The authors declare that they have no known competing financial interests or personal relationships that could have appeared to influence the work reported in this paper.

Acknowledgements

We wish to thank the National Research Foundation (NRF) of South Africa for funding through grant number CPRR23041794158. NM is a PhD bursar and SDO is a recipient of a postdoctoral fellowship award from the NRF. We also thank Stellenbosch University for funding and are also grateful to the South African Centre for High-Performance Computing, CHPC [www.chpc.ac.za] for resources.

Supplementary materials

Supplementary material associated with this article can be found, in the online version, at doi:10.1016/j.molstruc.2025.143220.

Data availability

Data will be made available on request.

References

[1] X. Xu, W. Wang, T. Liu, J. Zhao, Y. Wang, Heteroatomic-scale insight into the extraction selectivity of amic acid ligands and gallium and indium recovery from spent solar panels, Sep. Purif. Technol. 355 (Mar. 2025) 129639, https://doi.org/10.1016/J.SEPPUR.2024.129639.
[2] Shimojo Kojiro, Naganawa Hirochika, Noro Junji, Kubota Fukiko, Goto Masahiro, Extraction behavior and separation of lanthanides with a diglycol amic acid, Japan Society Analy. Chem. 23 (Dec. 2007).
[3] T. Hanada, K. Seo, W. Yoshida, A.T.N. Fajar, M. Goto, DFT-based investigation of Amic–Acid extractants and their application to the recovery of Ni and Co from spent automotive Lithium–Ion batteries, Sep. Purif. Technol. 281 (Jan. 2022), https://doi.org/10.1016/j.seppur.2021.119898.
[4] W. Yoshida, F. Kubota, Y. Baba, S.D. Kolev, M. Goto, Separation and recovery of scandium from sulfate Media by solvent extraction and polymer inclusion membranes with amic acid extractants, ACS Omega 4 (25) (Dec. 2019) 21122–21130, https://doi.org/10.1021/acsomega.9b02540.
[5] W. Yoshida, Y. Baba, F. Kubota, N. Kamiya, M. Goto, Extraction and stripping behavior of platinum group metals using an amic-acid-type extractant, J. Chem. Eng. Japan 50 (7) (2017) 521–526, https://doi.org/10.1252/jcej.16we335.
[6] Y. Baba, F. Kubota, N. Kamiya, M. Goto, Development of novel extractants with amino acid structure for efficient separation of nickel and cobalt from manganese ions, Ind. Eng. Chem. Res. 53 (2) (Jan. 2014) 812–818, https://doi.org/10.1021/ie403524a.
[7] Y. Baba, F. Kubota, N. Kamiya, M. Goto, Mutual separation of indium, gallium, and zinc with the amic acid-type extractant D2EHAG containing glycine and amide moieties, Solv. Extract. Res. Dev., Japan 23 (1) (2016) 9–18, https://doi.org/10.15261/serdj.23.9.
[8] P. Zhang, T. Yokoyama, T.M. Suzuki, and K. Inoue, 'The synergistic extraction of nickel and cobalt with a mixture of di(2-ethylhexyl) phosphoric acid and 5-dodecylsalicylaldoxime', 2001. [Online]. Available: www.elsevier.nlrlocaterhydromet.
[9] N.M. Harrison, 'An introduction to Density Functional theory', London, 2002.
[10] L. Noodleman, T. Lovell, W.-G. Han, T. Liu, R.A. Torres, and F. Himo, 'Density Functional Theory', 2005.
[11] G.M. Sheldrick, A short history of SHELX, Int. Union Crystallogr. (Jan. 01, 2008), https://doi.org/10.1107/S0108767307043930.
[12] J.L. Atwood and L.J. Barbour, 'Molecular graphics: from science to art', Jan. 2003. doi: 10.1021/cg020063o.
[13] L.J. Barbour, Product review X-Seed-A software tool for supramolecular crystallography, J. Supramol. Chem. (2001) [Online]. Available: http://www.povray.org.
[14] A.A. Badeji, Y. Liu, S.D. Oladipo, A.D. Osinubi, Computational insights into the mechanisms and origins of switchable selectivity in gold(i)-catalyzed annulation of ynamides with isoxazoles via 6π-electrocyclizations of azaheptatrienyl cations, RSC Adv. 13 (26) (Jun. 2023) 18025–18037, https://doi.org/10.1039/d3ra02839a.
[15] S.D. Oladipo, et al., Ni2+ and Cu2+ complexes of N-(2,6-dichlorophenyl)-N-mesityl formamidine dithiocarbamate structural and functional properties as CYP3A4 potential substrates, Sci. Rep. 13 (1) (Dec. 2023), https://doi.org/10.1038/s41598-023-39502-x.
[16] S.D. Oladipo, R.C. Luckay, Copper(II) complexes derived from naphthalene-based halogenated Schiff bases: synthesis, structural analysis, DFT computational studies and in vitro biological activities, New J. Chem. 48 (30) (Jul. 2024) 13276–13288, https://doi.org/10.1039/d4nj01621a.
[17] P.J. Hay, W.R. Wadt, Ab initio effective core potentials for molecular calculations. Potentials for K to Au including the outermost core orbitale, J. Chem. Phys. 82 (1) (1985) 299–310, https://doi.org/10.1063/1.448975.
[18] B.S. Jursic, D. Neumann, Preparation of N-acyl derivatives of amino acids from acyl chlorides and amino acids in the presence of cationic surfactants. A variation of the Schotten-Baumann method of benzoylation of amino acids, Synth. Commun. 31 (4) (2001) 555–564, https://doi.org/10.1081/SCC-100000582.
[19] A.P. Rajput and R.P. Gore, 'N-acylation in non-aqueous and aqueous medium-method of amide synthesis in non-peptide compounds', 2011. [Online]. Available: http://derpharmachemica.com/archive.html.
[20] M. Ebden, 'Gaussian processes: a quick introduction', Aug. 2015, [Online]. Available: http://arxiv.org/abs/1505.02965.
[21] F. Porcelli, F. Filippone, E. Colasante, G. Mattioli, Photoemission spectroscopy of organic molecules using plane wave/pseudopotential density functional theory and machine learning: a comprehensive and predictive computational protocol for isolated molecules, molecular aggregates, and organic thin films, J. Chem. Phys. 162 (24) (Jun. 2025), https://doi.org/10.1063/5.0272583.
[22] J. Foresman, 'Exploring chemistry with electronic structure methods', 1996. [Online]. Available: https://www.researchgate.net/publication/243763573.
[23] C.F. MacRae, I. Sovago, S.J. Cottrell, P.T.A. Galek, P. McCabe, E. Pidcock, M. Platings, G.P. Shields, J.S. Stevens, M. Towler, P.A. Wood, Mercury 4.0: from visualization to analysis, design and prediction, J. Appl. Crystallogr. 53 (Feb. 2020) 226–235, https://doi.org/10.1107/S1600576719014092.
[24] R.E.C. Torrejos, G.M. Nisola, H. SeongSong, L.A. Limjuco, C.P. Lawagon, K. J. Parohinog, S. Koo, J. Woo Han, W. Chung, Design of lithium selective crown ethers: synthesis, extraction and theoretical binding studies, Chem. Eng. J. 326 (2017) 921–933, https://doi.org/10.1016/j.cej.2017.06.005.
[25] G.M. Gasparini, G. Grossi, Long chain disubstituted aliphatic amides as extracting agents in industrial applications of solvent extraction, Solv. Extract. Ion Exchange 4 (6) (Jan. 1986) 1233–1271, https://doi.org/10.1080/07366298608917921.
[26] H. Sigel, B. Martin, Coordinating properties of the amide bond. Stability and structure of metal ion complexes of peptides and related ligands, Chem. Rev. (1982) [Online]. Available: https://pubs.acs.org/sharingguidelines.
[27] N. Condamines, C. Musikas, The extraction by N, N-dialkylamides.I. HNO_3 and other inorganic acids, Solv. Extract. Ion Exch. 6 (6) (1988) 1007–1034, https://doi.org/10.1080/07366298808917975.
[28] Arthur E. Martell, Robert D.Hancock, Chapter l Introductory Overview 1.1 Background to the Study of Complex-Formation in Aqueous Solutions, Springer Science + Business Media, New York, 1996.
[29] S.D. Oladipo, B. Omondi, C. Mocktar, Co(III) N,N′-diarylformamidine dithiocarbamate complexes: synthesis, characterization, crystal structures and biological studies, Appl. Organomet. Chem. 34 (5) (May 2020), https://doi.org/10.1002/aoc.5610.
[30] M.A. Halcrow, Jahn–Teller distortions in transition metal compounds, and their importance in functional molecular and inorganic materials, Chem. Soc. Rev. 42 (4) (Jan. 2013) 1784–1795, https://doi.org/10.1039/c2cs35253b.
[31] V. Amendola, M. Boiocchl, V. Brega, L. Fabbrizzi, L. Mosca, Octahedral copper(II) and tetrahedral copper(I) double-strand helicates: chiral self-recognition and redox behavior, Inorg. Chem. 49 (3) (Feb. 2010) 997–1007, https://doi.org/10.1021/ic9019684.
[32] J.I. Seeman, 'Recent studies on conformational analysis and steric effects', 1987.
[33] R.D. Hancock, A.E. Martell, Ligand design for selective complexation of metal ions in aqueous solution, Chem. Rev. 89 (8) (1989) 1875–1914, https://doi.org/10.1021/cr00098a011.
[34] P. Dierkes and P.W.N.M. Van Leeuwen, 'The bite angle makes the difference: a practical ligand parameter for diphosphine ligands', 1999.
[35] A. E. 1916-2003. (Arthur E. Martell, Metal Complexes in Aqueous Solutions, Plenum Press, New York, 2013.
[36] R.D. Hancock, L.J. Bartolotti, A DFT analysis of the effect of chelate ring size on metal ion selectivity in complexes of polyamine ligands, Polyhedron. 52 (Mar. 2013) 284–293, https://doi.org/10.1016/j.poly.2012.09.031.
[37] J.C.A. Boeyens, R.D. Hancock, G.J. Mcdougall, Empirical force-field calculations of strain-energy contributions to the thermodynamics of complex formation. Part II.

Further calculations on five- and six-membered rings, S. Afr. J. Chem. 32 (4) (1979) 103–106.

[38] K.V. Damu, H. Maumela, R.D. Hancock, J.C.A. Boeyens, S.M. Dobson, Structural and thermodynamic study of the effect of sterically hindering alkyl groups on complex stability, J. Chem. Soc. (10) (1991) 2717–2721, https://doi.org/10.1039/DT9910002717. *Dalton Transactions*.

[39] K. Omelchuk, P. Szczepański, A. Shrotre, M. Haddad, A. Chagnes, Effects of structural changes of new organophosphorus cationic exchangers on a solvent extraction of cobalt, nickel and manganese from acidic chloride media, RSC Adv. 7 (10) (2017) 5660–5668, https://doi.org/10.1039/c6ra21695a.

[40] L. Rulisek, Z. Havlas, Theoretical studies of metal ion selectivity. 1. DFT calculations of interaction energies of amino acid side chains with selected transition metal ions (Co^{2+}, Ni^{2+}, Cu^{2+}, Zn^{2+}, Cd^{2+}, and Hg^{2+}), J. Am. Chem. Soc. 122 (42) (Oct. 2000) 10428–10439, https://doi.org/10.1021/ja001265g.